Article

Structure

Directed Computational Evolution of Quorum-Quenching Lactonases from the Amidohydrolase Superfamily

Graphical Abstract

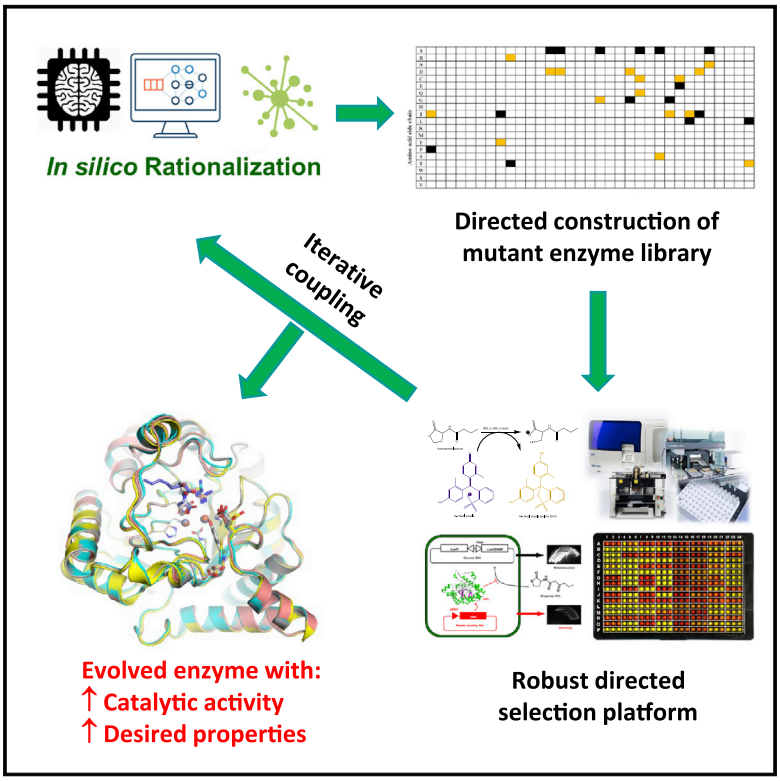

Highlights

- Generalizable computational protocol to identify engineering hotspots for enzyme
- Demonstrated utility of protocol for engineering GKL, a quorum-quenching lactonase
- Structures of Y99C and Y99P GKL mutants corroborated the utility of the protocol
- Protocol has built-in iteration capacity for future enhancement of enzyme engineering

Authors

Maybelle Kho Go, Li Na Zhao, Bo Xue, Shreyas Supekar, Robert C. Robinson, Hao Fan, Wen Shan Yew

Correspondence

fanh@bii.a-star.edu.sg (H.F.), bchyws@nus.edu.sg (W.S.Y.)

In Brief

Go et al. use *in silico* mutagenesis and substrate docking to rapidly identify hotspots on enzymes for enhanced substrate binding and overall catalysis. They demonstrate the utility of the protocol with a quorum-quenching *Geobacillus kaustophilus* lactonase, GKL, and solve two GKL mutant structures to provide rationalized explanations for the enhancement.

Go et al., 2020, Structure *28*, 1–8
June 2, 2020
https://doi.org/10.1016/j.str.2020.03.011

CellPress

Please cite this article in press as: Go et al., Directed Computational Evolution of Quorum-Quenching Lactonases from the Amidohydrolase Superfamily, Structure (2020), https://doi.org/10.1016/j.str.2020.03.011

Structure
Article

Directed Computational Evolution of Quorum-Quenching Lactonases from the Amidohydrolase Superfamily

Maybelle Kho Go,[1,2,5] Li Na Zhao,[3,5] Bo Xue,[1,2,5] Shreyas Supekar,[3] Robert C. Robinson,[4] Hao Fan,[3,*] and Wen Shan Yew[1,2,6,*]

[1]Department of Biochemistry, Yong Loo Lin School of Medicine, National University of Singapore, 8 Medical Drive, Singapore 117597, Singapore
[2]NUS Synthetic Biology for Clinical and Technological Innovation, 14 Medical Drive, Singapore 117599, Singapore
[3]Bioinformatics Institute, Agency for Science, Technology and Research, 30 Biopolis Street, Singapore 138671, Singapore
[4]Research Institute for Interdisciplinary Science, 3-1-1 Tsushima-naka, Kita-ku, Okayama 700-8530, Japan
[5]These authors contributed equally
[6]Lead Contact
*Correspondence: fanh@bii.a-star.edu.sg (H.F.), bchyws@nus.edu.sg (W.S.Y.)
https://doi.org/10.1016/j.str.2020.03.011

SUMMARY

In this work, we present a generalizable directed computational evolution protocol to effectively reduce the sequence space to be explored in rational enzyme design. The protocol involves *in silico* mutation modeling and substrate docking to rapidly identify mutagenesis hotspots that may enhance an enzyme's substrate binding and overall catalysis. By applying this protocol to a quorum-quenching *Geobacillus kaustophilus* lactonase, GKL, we generated 1,881 single mutants and docked high-energy intermediates of nine acyl homoserine lactones onto them. We found that Phe28 and Tyr99 were two hotspots that produced most of the predicted top 20 mutants. Of the 180 enzyme-substrate combinations (top 20 mutants × 9 substrates), 51 (28%) exhibited enhanced substrate binding and 22 (12%) had better overall activity when compared with wild-type GKL. X-ray crystallographic studies of Y99C and Y99P provided rationalized explanations for the enhancement in enzyme function and corroborated the utility of the protocol.

INTRODUCTION

Antibiotic resistance is rising to dangerously high levels in all parts of the world. New resistance mechanisms are emerging and spreading globally, threatening our ability to treat common infectious diseases. A growing list of infections such as pneumonia, tuberculosis, blood poisoning, gonorrhea, and foodborne illness are becoming more difficult, and sometimes impossible, to treat as antibiotics become less effective (Ferri et al., 2017). Traditionally, antibiotics target biological pathways in the bacteria that are integral to the organism's survival. Due to selection pressures, it is not surprising that microbes have evolved to resist the effects of antibiotics that have been used for the past 80 years (Spellberg, 2014). The modulation and perturbation of other biological pathways in microbes that are not integral to their survival, such as antivirulence strategies, seems to be an attractive alternative to combat antimicrobial resistance (Stadler and Dersch, 2016).

Quorum sensing is a communication method for microbes but is not an integral part for their survival. It is responsible for the virulence and pathogenicity of pathogenic bacteria. Recent studies show that modulation and perturbation of quorum-sensing pathways is an effective antimicrobial strategy (Camilli and Bassler, 2006). Disruption of quorum-sensing pathways, or quorum quenching, does not exert the selective pressure that always results in the development of antimicrobial resistance. Among the various quorum-quenching strategies, enzymatic degradation of messenger small molecules, such as *N*-acyl-homoserine lactones (AHLs), attracts much attention due to its versatility and easy implementation. Consequently, enzymes with quorum-quenching capability are being extensively exploited to unlock their potential as therapeutic biomolecules (Dong et al., 2001).

The amidohydrolase superfamily of enzymes consists of over 36,000 members bearing a conserved mononuclear or binuclear metal center within a $(\beta/\alpha)_8$-barrel structural scaffold (Akiva et al., 2014). This superfamily was first reported by Holm and Sander (1997) and has since expanded to cover more than 30 reactions involving a diverse range of enzymatic activities, including the degradation of quorum-sensing AHLs (Afriat et al., 2006). Among this superfamily are AHLs that catalyze ring-opening hydrolysis reactions on diverse AHL substrates. We have previously characterized a few such lactonases (Chow et al., 2009, 2010). One of these was a lactonase from a thermophilic organism, *Geobacillus kaustophilus*, which exhibited high-level expression, solubility, and thermostability (abbreviated as GKL hereafter). By creating a robust and tunable directed evolution platform for mutant library screening, we successfully identified several GKL mutants with enhanced quorum-quenching activities against a broad range of AHLs (Chow et al., 2010). In addition, we also provided structural evidence of a productive active-site architecture in GKL (Xue et al., 2013).

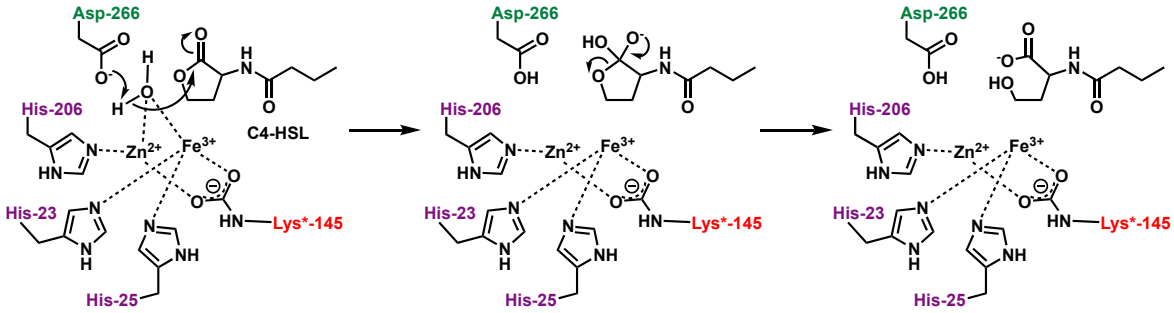

Figure 1. Proposed Catalytic Mechanism for GKL

The binuclear metal ions are indicated as Fe^{3+} and Zn^{2+}, respectively. Hydrolysis of the AHL substrate by GKL is catalyzed by nucleophilic attack of the hydroxide on the *si* face of the lactone ring of the AHL.

The structure of GKL consists of a $(\beta/\alpha)_8$ barrel, and it has two metal ion-binding sites within its active site, which is located at the C-terminal end of the barrel (Chow et al., 2010; Xue et al., 2013). Of the two sites, the more solvent-occluded α site and the more solvent-exposed β site require an Fe^{3+} and a Zn^{2+}, respectively for wild-type GKL to function as a lactonase. Substitution of the β cation by Mn^{2+} can be tolerated by certain GKL mutants, whereas substitution by other common metal ions (Mg^{2+}, Ca^{2+}, Co^{2+}, Ni^{2+}, and Cu^{2+}) inactivates the enzyme (Chow et al., 2010). The proposed catalytic mechanism for GKL (shown in Figure 1) involves a binuclear metal center with a bridging hydroxide; this hydroxide serves as a nucleophile during catalysis to hydrolyze an ensuing lactone substrate (AHL). The lactone ring of the AHL substrate becomes polarized upon close proximity to the binuclear metal ions, facilitating the nucleophilic attack by the hydroxide. This proposed mechanism is similar to that of AiiA, a lactonase from *Bacillus thuringiensis* (Liu et al., 2008; Momb et al., 2008). Many amino acid residues lining the active center are involved in substrate binding (see below), whereas residue Asp266 acts as a proton shuttle between the attacking nucleophilic hydroxide and the leaving group. Consequently, an Asp266-to-Asn mutation invariably inactivates the enzyme (Chow et al., 2010; Xue et al., 2013).

In the current study, we developed a generalizable computational protocol with an iterative capacity to facilitate the identification of enzyme mutants that are catalytically more competent than the wild type. The protocol involves an exhaustive generation of point mutations lining an enzyme's active site and mutant evaluation based on substrate docking. As a case study, we applied this protocol to GKL and demonstrated its capability to achieve rapid and robust identification of GKL mutants with enhanced lactonase activity (vis-a-vis catalytic efficiency and broadened substrate specificity) with respect to the wild-type enzyme.

RESULTS

Computational Design of GKL Mutants

Docking against GKL Crystal Structures

The crystal structures for the wild-type GKL (WT), E101G/R230C mutant GKL (GC mutant), and E101G/R230C/D266N mutant GKL (GCN mutant) were obtained from the Protein Data Bank (PDB: 4H9U, 4H9V, and 4H9X, respectively) (Xue et al., 2013). The five missing residues (E101 to A105) in the β3 loop of GC and GCN were built with Modeller 9.14 (Sali and Blundell, 1993), and neighboring side chains were predicted by PLOP (Protein Local Optimization Program) (Sherman et al., 2006). We docked substrates in their high-energy intermediate (HEI) states into the catalytic sites of the crystal structures of the WT, GC, and GCN mutants. The modeling and docking against the crystal structures of the WT, GC, and GCN mutants were used to evaluate our computational methods and to establish an automated pipeline for mutation predictions.

Docking against GKL Point Mutants

Molecular docking of substrates to predicted mutant structures was used to evaluate effects of point mutations on catalytic activity with respect to the WT. Considering residues within 12 Å from the metal ions and excluding the six metal-binding residues (H23, H25, H178, H206, D266, and an *N*-carboxylated lysine [KCX145]) in the GKL WT structure, in total 99 residues were included in point mutation predictions. Each residue was substituted into 19 other residue types independently. The side-chain conformations of the mutated residue and neighboring residues within 10-Å distance were predicted using the "side chain prediction" protocol in PLOP (Sherman et al., 2006). For each of the 1881 (99 × 19) GKL point mutant structures computed by the side-chain prediction method in PLOP, the HEI states of the nine substrates were docked into the predicted catalytic site. The docking energies for the nine substrates were calculated, averaged, and ranked across the 1,881 mutants. A total of 40 mutants were chosen for experimental testing: 20 mutants with the best docking energies and 20 with the worst docking energies (see Table S1). The 20 mutants with the best docking energies are F28C/G/Q/S/T/V, P71K, Y99A/C/P/G/I/K/L/N/S/T/V/Q, and Y100Q. The 20 mutants with the worst docking energies are T183C, G205R, I233F, Q234D, G235W, V237E/I/L, S264W, V268M/W/Y, T277N, L278Q/W/Y, F282M, and M286E/H/R. The locations of these residues are indicated in Figure 2.

Biochemical Characterization of Wild-Type GKL and Mutants

Wild-type GKL was active against all the substrates tested, with catalytic efficiency (k_{cat}/K_M) ranging from 2.6×10^2 M^{-1} s^{-1} for C4-HSL to $\sim 1.0 \times 10^7$ M^{-1} s^{-1} for C10- and C12-HSLs as well as their 3-oxo derivatives (Figure 2 and Table S2). Substrate

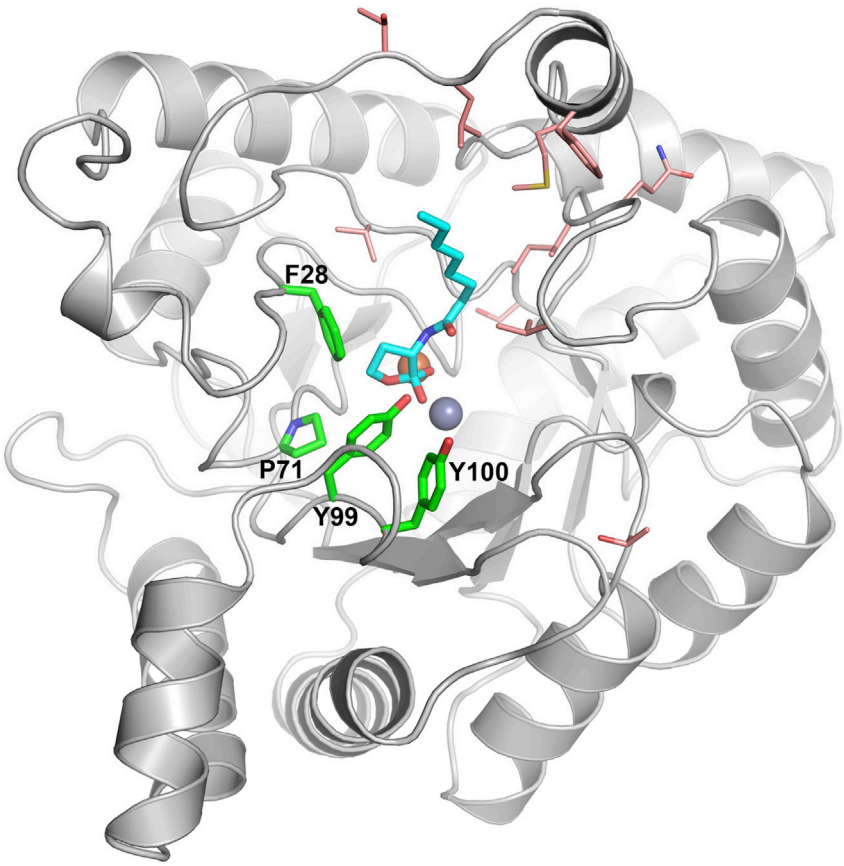

Figure 2. Residue Selection for *In Silico* Mutagenesis on Wild-Type GKL (Gray Cartoon)

The best and worst 20 docking energy scorers are shown as thick sticks and colored green and pink, respectively. A docked C8-HSL HEI (cyan) is shown as an example. Cations at the active center are shown as spheres.

turnover was slow, with k_{cat} for most of the substrates in the order of 1.0×10^{-1} s^{-1}. The K_M values were in the micromolar and nanomolar range for shorter- and longer-chain AHLs, respectively. These values define the upper boundaries of the dissociation constants for GKL-substrate complexes, and are good approximations for GKL's substrate-binding affinity under slow substrate turnover. It is therefore safe to conclude from Figure 3 that GKL's substrate binding and overall catalytic efficiency correlate positively with the chain length of the AHLs, and are not affected significantly by the presence of the 3-oxo group on the AHLs.

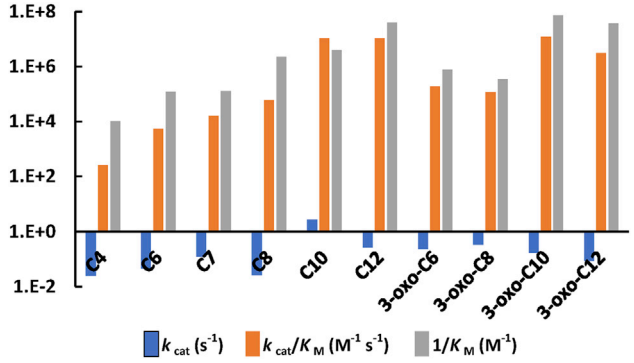

Figure 3. Overall Catalytic Efficiency of GKL against Different AHLs

Activity of 20 Single Mutants with Best Docking Energies of Substrates

All 20 mutants had comparable protein yields when compared with the wild type, out of which 15 mutants retained activity in varying degrees. Most of the mutants that exhibited the best docking energies are based on two residues, Tyr99 (12 mutants) and Phe28 (6 mutants), followed by Pro71 (1 mutant) and Tyr100 (1 mutant). The minimum distances between these residues and the tetrahedral carbon of the C8-HSL HEI are 3.1, 4.1, 5.9, and 6.6 Å, respectively (Figure 2).

The Phe28 mutants showed varying degrees of improvement and deterioration. All except F28V had better catalytic efficiency (higher k_{cat}/K_M values by up to 50-fold) against shorter-chain AHLs (C4 to C8) when compared with the wild type, which can be attributed to improved binding (increase of $1/K_M$ values by 2- to 20-fold), enhanced turnover rate of the substrates (increase of k_{cat} values by up to 13-fold), or a combination of both (Figure 4). They were, however, invariably worse against longer-chain and 3-oxo-substitued AHLs, with drastic reduction in their substrate binding and turnover (Table S2).

P71K and Y100Q showed marginal improvement against specific substrates (Table S2). Unfortunately, the overall activity of the enzymes toward the range of substrates showed that mutating these positions became a detriment rather than an improvement of the enzyme.

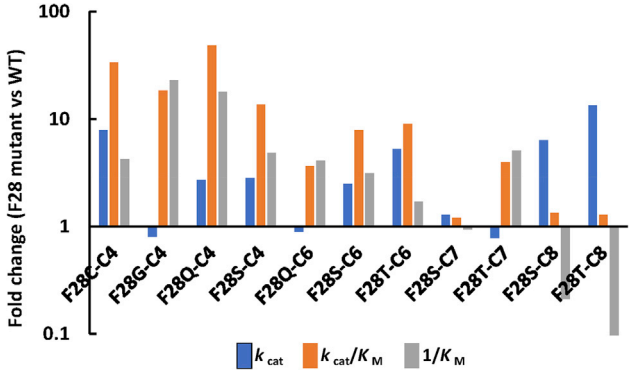

Figure 4. Phe28 Mutants with Enhanced Catalytic Activities

The Phe28 mutant-AHL (C4-C8) combinations are indicated below the bars.

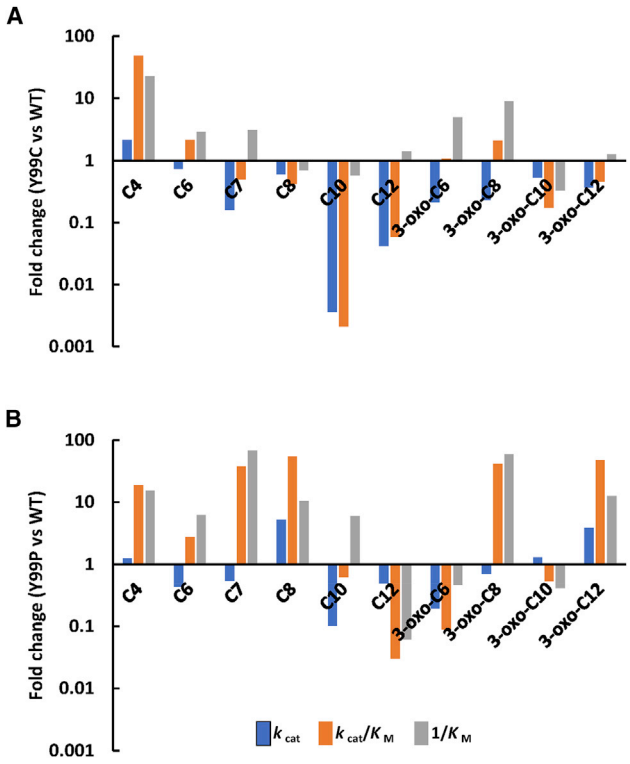

Figure 5. Tyr99 Mutants with Enhanced Catalytic Activities
Fold change in substrate turnover, catalytic efficiency, and substrate binding for (A) Y99C and (B) Y99P compared with wild-type GKL.

There were 12 Tyr99 mutants that showed the best docking energies. Out of these 12 mutants, eight (Y99G, Y99I, Y99K, Y99L, Y99N, Y99Q, Y99S, and Y99T) were either inactive or became less active than the wild type against the different substrates; two (Y99A and Y99V) were better against C4-HSL (due to enhanced substrate binding) but not the rest of the substrates. In stark contrast, the remaining two mutants on the list, Y99C and Y99P, not only retained activity against all substrates but also showed enhanced activities against several of the substrates when compared with the wild type (Figure 5 and Table S2). Binding affinity of the substrates either remained unchanged or was improved (up to 60-fold) and in many cases was the driving force for the enhanced activities. For most of the substrates, their turnover rates by these two mutants were only mildly reduced (2- to 5-fold) with reference to the wild type, with C10-HSL being an exception for both mutants (10- to 100-fold reduction) and C12-HSL for Y99C only (17-fold reduction). Given their superior activities, these two mutants were further characterized by X-ray crystallography.

Activity of Single Mutants with the Worst Docking Energies

The 20 mutants with the worst docking energies reside on 12 residues, most of which are in the region that interacts with the acyl-chain portion of the AHLs (Figure 2). As none of the 20 mutants showed activity above the background hydrolysis of AHLs, we were unable to obtain kinetic parameters and use the $1/K_M$ values to verify whether impaired substrate binding is indeed the reason behind the loss of activity for these mutants. Since these inactive mutants were of no interest to quorum quenching, they were not further characterized.

Structures of Y99P and Y99C Mutants

The structures of Y99P, Y99P/D266N, and Y99C/D266N were refined against data to resolutions of 2.16, 1.80, and 1.73 Å, respectively (Table 1). Both Y99P/D266N and Y99C/D266N were co-crystallized with 3-oxo-C8-HSL and soaked with a cryoprotectant containing 3-oxo-C8-HSL prior to data collection. However, only one copy of Y99P/D266N (chain A) out of the four in the crystallographic asymmetric unit had clear electron density for an oxo-C8-HSL, whereas none of the four copies of Y99C/D266N showed evidence of ligand binding, which is consistent with Y99P's better binding affinity against 3-oxo-C8-HSL than Y99C (Figure 5 and Table S2). There are no significant overall structural changes in these mutants when compared with the wild-type GKL (Figure 6). The most prominent differences near the catalytic center of the enzyme are manifested by the β2, β3, and β7 loops (Figure 6), which could be attributed to the Y99P/C mutations and substrate binding. Like wild-type GKL, the inactivating D266N mutation on a Y99P background does not alter the conformations of these loops (Figure S3). One unique feature of the Y99P mutant is the shift of the β2 loop, caused by the steric hindrance between the side chains of the newly introduced proline and Asp73 (Figure 6). Such an effect is clearly non-existent in the Y99C mutant, and we postulate that the same is true for the rest of the Tyr99 mutants tested.

DISCUSSION

In the past decade, great effort has been made to improve the activity and substrate selectivity of enzymes (Arnold, 2018; Badenhorst and Bornscheuer, 2018). Computational methods have been developed to generate all possible mutations of target enzymes to complement experimental approaches for the identification of desirable variants with improved properties and meet the practical needs (Wu et al., 2019). In this study, we constructed an automated computational pipeline that combines protein structure modeling and molecular docking to provide structure-based guidance for a more efficient and accurate enzyme engineering workflow. In particular, we sought to establish a general protocol for further enhancing the activity of a thermostable quorum-quenching lactonase by reliably identifying point mutants with improved catalytic activities across a broad range of AHLs.

Wild-type GKL exhibited promiscuous activities toward many AHLs while favoring AHLs with longer acyl chains. For translational use of these quorum-quenching enzymes as effective antivirulence therapeutic agents, it is necessary to further enhance the catalytic activities of these lactonases, particularly toward AHLs with shorter acyl-chain lengths. Of the four potential positions identified by docking, the replacement of Phe28 with cysteine, glycine, glutamine, serine, or threonine produced enzymes with improved binding and catalysis toward AHLs with shorter acyl chains (C4 to C8); however, catalytic enhancement was not observed for AHL substrates with longer acyl chains and 3-oxo substitutions (Table S2). Phe28 is surrounded by several key aromatic residues including Tyr30, Tyr99, His25,

Table 1. Data Collection and Refinement Statistics

	Y99P	Y99P/D266N + 3-oxo-C8-HSL	Y99C/D266N
PDB ID	6JSS	6JST	6JSU
Wavelength (Å)	0.9537	1.0000	0.9537
Resolution range (Å)	19.71–2.16 (2.24–2.16)	19.99–1.73 (1.79–1.73)	19.87–1.80 (1.86–1.80)
Space group	P 1	P 1	P 1 2_1 1
Unit cell (*a*, *b*, *c* [Å]; α, β, γ [°])	51.49, 51.65, 135.29; 91.83, 91.49, 95.78	50.99, 51.19, 134.47; 90.99, 91.33, 96.33	47.6, 157.49, 50.62; 90, 117.06, 90
Total reflections	159,846 (15,201)	521,489 (30,192)	431,208 (42,329)
Unique reflections	72,639 (7,017)	133,194 (8,687)	60,788 (6,015)
Multiplicity	2.2 (2.2)	3.9 (3.5)	7.1 (7.0)
Completeness (%)	97.9 (94.6)	93.8 (61.3)	99.2 (98.4)
Mean $I/\sigma(I)$	12.3 (1.8)	34.6 (4.7)	22.9 (4.4)
Wilson *B* factor	26.5	16.0	23.7
R_{merge}	0.112 (0.468)	0.182 (0.417)	0.0561 (0.351)
R_{meas}	0.149 (0.634)	0.211 (0.485)	0.061 (0.379)
R_{pim}	0.098 (0.426)	0.106 (0.247)	0.0225 (0.140)
$CC_{1/2}$	0.981 (0.710)	0.972 (0.743)	0.999 (0.957)
CC*	0.995 (0.911)	0.993 (0.923)	1.000 (0.989)
Reflections used in refinement	72,638 (7015)	133193 (8677)	60,719 (6012)
Reflections used for R_{free}	3,626 (379)	6,521 (394)	3,231 (305)
R_{work}	0.175 (0.275)	0.219 (0.264)	0.160 (0.214)
R_{free}	0.229 (0.350)	0.264 (0.326)	0.190 (0.256)
CC_{work}	0.949 (0.851)	0.847 (0.779)	0.970 (0.940)
CC_{free}	0.912 (0.697)	0.818 (0.607)	0.960 (0.906)
No. of non-hydrogen atoms in	10,876	10,942	5,547
Macromolecules	10,152	10,152	5,074
Ligands	12	28	6
Solvent	712	762	467
Protein residues	1,304	1,304	650
RMS (bonds, Å)	0.008	0.007	0.007
RMS (angles, °)	0.90	0.91	0.84
Ramachandran favored (%)	96.93	97.09	98.27
Ramachandran allowed (%)	3.07	2.91	1.73
Ramachandran outliers (%)	0.00	0.00	0.00
Rotamer outliers (%)	0.19	0.19	0.00
Clashscore	4.98	6.01	2.09
Average *B* factor (Å^2)	30.10	30.59	31.43
Macromolecules	29.83	30.38	30.65
Ligands	25.22	35.33	20.96
Solvent	34.00	33.14	40.06
No. of TLS groups	26	29	19

Statistics for the highest-resolution shell are shown in parentheses. RMS, root-mean-square; TLS, translation/libration/screw.

and Trp271, and interacts with them extensively through hydrophobic interaction and π-π stacking; Phe28 also interacts with the lactone ring of the bound AHLs (Figure S4). Substitution of Phe28 would have profound effects on the rigidity of the catalytic core, on the binding affinity, and on the orientation of the bound substrates. The reduced rigidity of the catalytic core and the enlarged substrate-binding pocket (due to substitutions by smaller, non-aromatic side chains) in the Phe28 mutants would allow a higher degree of freedom, or reduced entropy cost, for the lactone ring to reach the most favorable orientation for hydrolysis to occur. For shorter-chain AHLs, the lactone ring takes up a larger portion in overall substrate binding; consequently, more pronounced differences in substrate binding would be expected between the Phe28 mutants and the wild type. Indeed, such an explanation does seem to corroborate with the majority of the kinetic data in Figure 3 and Table S2, in which binding (and activity) is increased toward AHLs with shorter acyl chains and decreased toward AHLs with longer

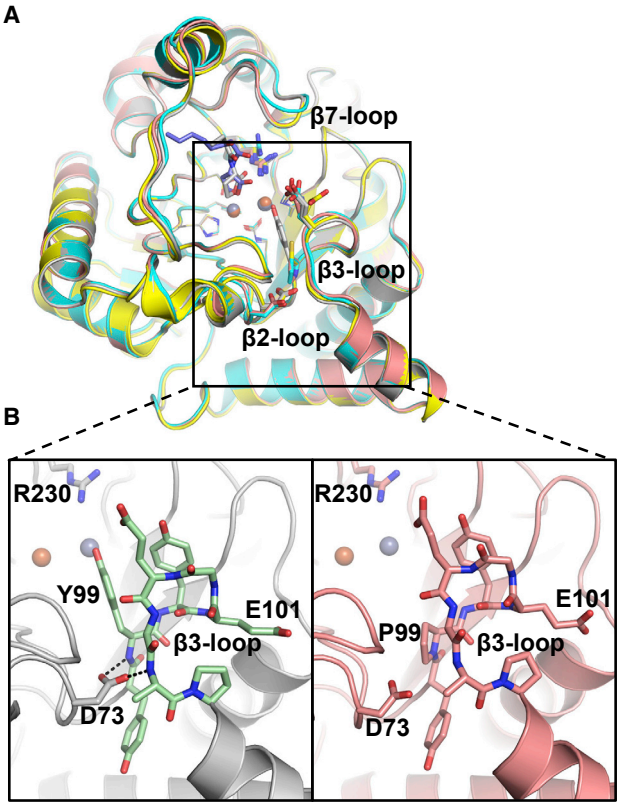

Figure 6. Structural Superposition of Y99 Mutants with Wild-type GKL

(A) Structures of Y99P (pink) and Y99P/D266N (cyan), with bound 3-oxo-C8-HSL (blue) and Y99C/D266N (yellow) overlaid onto wild-type GKL (gray, PDB: 4H9U). Bound C4-HSL (gray) in the structure of D266N mutant (PDB: 3OJG) is shown to highlight the difference in the orientation of the lactone rings between 3-oxo-C8-HSL and C4-HSL.

(B) Y99P causes the loss of hydrogen bonds (dashed lines, left panel) between D73 and the β3 loop (highlighted green for the wild type), leading to enhanced flexibility of the β3 loop.

acyl chains. There are observed exceptions to the overall trend, particularly F28V; as they did not show the desired enhanced activities, no further studies were carried out on them.

Another "beneficial" position identified by docking is Tyr99 (also see Figures S6 and S7 for efficacy of computational predictions). Incidentally, this residue has been shown to be greatly perturbed upon substrate binding. As has been reported previously (Xue et al., 2013), when the catalytic center was occupied by C4-HSL, Tyr99 was concomitantly displaced away from it; the removal of the electron-rich hydroxyl group of Tyr99 from the β cation by such a displacement would enhance the polarization effect of the lactone ring by the β cation. To avoid steric hindrance to the movement of Tyr99, the β3 loop, onto which both Tyr99 and Glu103 reside, had to reorient itself away from its original conformation, resulting in increased flexibility and partial loop disorder. In the present study, the 3-oxo-C8-HSL bound to Y99P/D266N resembles the C4-HSL bound to D266N; however, there is no induced positional displacement of residue 99 upon ligand binding, as the Y99P/C mutations eliminate the need for such a movement. Consequently, the β3 loop remains ordered even when the substrate is positioned within the catalytic center. Nonetheless, the movement of the β3 loop becomes less restricted due to the removal of the Tyr99 side chain in the Y99P/C mutants, which is best demonstrated by the different rotamer conformations of the side chain of Glu103 (Figure S3).

It is intriguing to observe how the 12 mutations at the same Y99 position (Y99A/C/P/G/I/K/L/N/S/T/V/Q) differentially affected GKL's catalytic activities. The observed differences among themselves might be partly attributed to the alterations of the aromatic interaction network and the substrate-binding pocket, as similarly observed in the various Phe28 substitutions; however, additional factors may also contribute to their different catalytic activities. Substitution of Tyr99 with other amino acid residues may or may not affect dimerization and thermostability of the enzyme, and there seems to be no correlation between these physical properties and the activity of the enzyme (Table S3). Based on the available structures of Y99C/D266N and Y99P/D266N, we hypothesize that, on top of the expected effects of aromatic side-chain removal, Y99C and Y99P could have contributed to the observed catalytic enhancements through other mechanisms. We have previously demonstrated that charge transfer existed between the α cation (Fe^{3+}) and the hydroxyl group of Tyr99, which are 6.2 Å apart. Of the 12 mutations tested, the Y99C mutation would be most well positioned to maintain this charge-transfer phenomenon. Although this mutation resulted in a larger separation (8.8 Å) between the Fe^{3+} and the sulfhydryl group of Cys99, the easier deprotonation of the sulfhydryl group of Cys99, as compared with the hydroxyl group of Tyr99, would compensate for the increased distance between the two charge-transfer components (vis-a-vis Cys99 and the Fe^{3+} α cation). For Y99P, we rationalize that the steric effects exerted onto Asp73 in the β2 loop resulted in conformational changes in this loop that could propagate to other parts of the enzyme and influence substrate binding allosterically. A direct consequence of changes in the β2-loop conformation is the loss of hydrogen bonds between Asp73 and two backbone nitrogen atoms located at the two ends of the β3 loop, thus granting more freedom to the β3 loop in its movement (Figure 6). As has been demonstrated previously by the E101G/R230C mutant, enhancing the mobility of the β3 loop does make the enzyme catalytically more active. For substrate binding, although a comparison between 3-oxo-C8-HSL and C4-HSL is strictly speaking not fair due to their differences in alkyl chain length and 3-oxo-substitution, further rationalization suggests that the lactone ring of the 3-oxo-C8-HSL bound onto the Y99P/D266N double mutant is indeed in a more "catalytically productive" orientation, similar to what had been observed for the E101G/R230C mutant (Xue et al., 2013); the scissile bond of the lactone ring is "more orthogonally" oriented toward the attacking nucleophilic OH^- group, as compared with that of the C4-HSL substrate bound within the active site of the D266N single mutant; specifically, the nucleophilic attack angle between the plane of the lactone ring (defined by the scissile bond, the carbonyl carbon, and the oxo-ring prior to the formation of the tetrahedral intermediate) and the nucleophile (defined vectorially by the attacking OH^- group and the carbonyl carbon) are 28° from the *si* face of the ring and 22° from the *re* face of the ring, respectively, for Y99P/D266N-bound 3-oxo-C8-HSL and D266N-bound C4-HSL.

In summary, we have developed a highly iterative modeling and docking strategy to effectively screen *in silico* the binding of a series of chemically related substrates onto a large collection of singly mutated enzymes. Identified mutagenesis hotspots, in many cases, resulted in engineered enzymes with enhanced catalytic efficiency and substrate-binding profiles. X-ray crystallographic structures of two of the best-performing mutants provided plausible mechanistic explanations for their enhancement in catalysis. We note that the correlations between catalytic efficiency and docking scores of individual substrates are weak (Figures S6 and S7) and it remains difficult to predict the efficacy of an individual substrate solely based on its docking score. However, the averaged docking scores measured in this study serve well for the high-throughput directed computational evolution protocol, which while producing some false positives accounts for all the improved variants, which can then be further tested by more accurate computational or experimental strategies. Future work should be directed toward developing algorithms to better discern the subtle differences between the many possible mutations for the same positional hotspot so that the number of mutants put into experimental verification can be further reduced reliably. The combinatory effects of different mutations on catalysis represent another area that needs further improvement. Success in identifying double, triple, or even higher-ordered combination of mutations would allow us to access an enzyme sequence landscape that is several orders of magnitude larger than the current one, and that could increase the reliability and robustness in engineering desired enzymes with purposeful function.

STAR★METHODS

Detailed methods are provided in the online version of this paper and include the following:

- KEY RESOURCES TABLE
- LEAD CONTACT AND MATERIALS AVAILABILITY
- EXPERIMENTAL MODEL AND SUBJECT DETAILS
- METHOD DETAILS
  - Construction of Virtual Chemical Library
  - Materials
  - GKL Point Mutant Prediction and Molecular Docking
  - Overexpression and Purification of GKL
  - Biophysical Characterization of GKL
  - Kinetic Assays of Lactonase Activity
  - Crystallization and Structure Solution of GKL Mutants
- QUANTIFICATION AND STATISTICAL ANALYSIS
- DATA AND CODE AVAILABILITY
  - Data Resources
  - Software Availability

SUPPLEMENTAL INFORMATION

Supplemental Information can be found online at https://doi.org/10.1016/j.str.2020.03.011.

ACKNOWLEDGMENTS

This work was supported by the National Research Foundation Singapore (to W.S.Y.) and by the Biomedical Research Council of A*STAR (to H.F.). This research was undertaken in part using the MX1 and MX2 beamlines at the Australian Synchrotron, part of ANSTO, and made use of the Australian Cancer Research Foundation detector.

AUTHOR CONTRIBUTIONS

Conceptualization, H.F. and W.S.Y.; Formal Analysis, L.N.Z., S.S., and H.F.; Investigation, M.K.G. and B.X.; Writing – Original Draft, M.K.G., L.N.Z., B.X., S.S., R.C.R., H.F., and W.S.Y.; Writing – Review & Editing, M.K.G., L.N.Z., B.X., S.S., R.C.R., H.F., and W.S.Y.

DECLARATION OF INTERESTS

The authors declare no competing interests.

Received: July 22, 2019
Revised: March 2, 2020
Accepted: March 23, 2020
Published: April 21, 2020

REFERENCES

Adams, P.D., Afonine, P.V., Bunkóczi, G., Chen, V.B., Davis, I.W., Echols, N., Headd, J.J., Hung, L.W., Kapral, G.J., Grosse-Kunstleve, R.W., et al. (2010). PHENIX: a comprehensive Python-based system for macromolecular structure solution. Acta Crystallogr. D Biol. Crystallogr. *66*, 213–221.

Afriat, L., Roodveldt, C., Manco, G., and Tawfik, D.S. (2006). The latent promiscuity of newly identified microbial lactonases is linked to a recently diverged phosphotriesterase. Biochemistry *45*, 13677–13686.

Akiva, E., Brown, S., Almonacid, D.E., Barber, A.E., Custer, A.F., Hicks, M.A., Huang, C.C., Lauck, F., Mashiyama, S.T., Meng, E.C., et al. (2014). The structure-function linkage database. Nucleic Acids Res. *42*, D521–D530.

Aragão, D., Aishima, J., Cherukuvada, H., Clarken, R., Clift, M., Cowieson, N.P., Ericsson, D.J., Gee, C.L., Macedo, S., Mudie, N., et al. (2018). MX2: a high-flux undulator microfocus beamline serving both the chemical and macromolecular crystallography communities at the Australian Synchrotron. J. Synchrotron Radiat. *25*, 885–891.

Arnold, F.H. (2018). Directed evolution: bringing new chemistry to life. Angew. Chem. Int. Ed. *57*, 4143–4148.

Badenhorst, C.P.S., and Bornscheuer, U.T. (2018). Getting momentum: from biocatalysis to advanced synthetic biology. Trends Biochem. Sci. *43*, 180–198.

Camilli, A., and Bassler, B.L. (2006). Bacterial small-molecule signaling pathways. Science *311*, 1113–1116.

Chapman, E., and Wong, C.-H. (2002). A pH sensitive colorometric assay for the high-throughput screening of enzyme inhibitors and substrates: a case study using kinases. Bioorg. Med. Chem. *10*, 551–555.

Chen, V.B., Arendall, W.B., Headd, J.J., Keedy, D.A., Immormino, R.M., Kapral, G.J., Murray, L.W., Richardson, J.S., and Richardson, D.C. (2010). MolProbity: all-atom structure validation for macromolecular crystallography. Acta Crystallogr. D Biol. Crystallogr. *66*, 12–21.

Chow, J.Y., Wu, L., and Yew, W.S. (2009). Directed evolution of a quorum-quenching lactonase from *Mycobacterium avium* subsp. *paratuberculosis* K-10 in the amidohydrolase superfamily. Biochemistry *48*, 4344–4353.

Chow, J.Y., Xue, B., Lee, K.H., Tung, A., Wu, L., Robinson, R.C., and Yew, W.S. (2010). Directed evolution of a thermostable quorum-quenching lactonase from the amidohydrolase superfamily. J. Biol. Chem. *285*, 40911–40920.

Cowieson, N.P., Aragao, D., Clift, M., Ericsson, D.J., Gee, C., Harrop, S.J., Mudie, N., Panjikar, S., Price, J.R., Riboldi-Tunnicliffe, A., et al. (2015). MX1: a bending-magnet crystallography beamline serving both chemical and macromolecular crystallography communities at the Australian Synchrotron. J. Synchrotron Radiat. *22*, 187–190.

Dong, Y.H., Wang, L.H., Xu, J.L., Zhang, H.B., Zhang, X.F., and Zhang, L.H. (2001). Quenching quorum-sensing-dependent bacterial infection by an N-acyl homoserine lactonase. Nature *411*, 813–817.

Emsley, P., Lohkamp, B., Scott, W.G., and Cowtan, K. (2010). Features and development of Coot. Acta Crystallogr. D Biol. Crystallogr. *66*, 486–501.

Fan, H., Hitchcock, D.S., Seidel, R.D., Hillerich, B., Lin, H., Almo, S.C., Sali, A., Shoichet, B.K., and Raushel, F.M. (2013). Assignment of pterin deaminase activity to an enzyme of unknown function guided by homology modeling and docking. J. Am. Chem. Soc. *135*, 795–803.

Ferri, M., Ranucci, E., Romagnoli, P., and Giaccone, V. (2017). Antimicrobial resistance: a global emerging threat to public health systems. Crit. Rev. Food Sci. Nutr. *57*, 2857–2876.

Go, M.K., Chow, J.Y., and Yew, W.S. (2018). Directed evolution of quorum-quenching enzymes: a method for the construction of a directed evolution platform and characterization of a quorum-quenching lactonase from *Geobacillus kaustophilus*. Methods Mol. Biol. *1673*, 311–323.

Hermann, J.C., Ghanem, E., Li, Y., Raushel, F.M., Irwin, J.J., and Shoichet, B.K. (2006). Predicting substrates by docking high-energy intermediates to enzyme structures. J. Am. Chem. Soc. *128*, 15882–15891.

Hermann, J.C., Marti-Arbona, R., Fedorov, A.A., Fedorov, E., Almo, S.C., Shoichet, B.K., and Raushel, F.M. (2007). Structure-based activity prediction for an enzyme of unknown function. Nature *448*, 775–779.

Holm, L., and Sander, C. (1997). An evolutionary treasure: unification of a broad set of amidohydrolases related to urease. Proteins *28*, 72–82.

Kabsch, W. (2010). XDS. Acta Crystallogr. D Biol. Crystallogr. *66*, 125–132.

Kuntz, I.D., Blaney, J.M., Oatley, S.J., Langridge, R., and Ferrin, T.E. (1982). A geometric approach to macromolecule-ligand interactions. J. Mol. Biol. *161*, 269–288.

Liu, D., Momb, J., Thomas, P.W., Moulin, A., Petsko, G.A., Fast, W., and Ringe, D. (2008). Mechanism of the quorum-quenching lactonase (AiiA) from *Bacillus thuringiensis*. 1. Product-bound structures. Biochemistry *47*, 7706–7714.

McCoy, A.J., Grosse-Kunstleve, R.W., Adams, P.D., Winn, M.D., Storoni, L.C., and Read, R.J. (2007). Phaser crystallographic software. J. Appl. Crystallogr. *40*, 658–674.

McPhillips, T.M., McPhillips, S.E., Chiu, H.-J., Cohen, A.E., Deacon, A.M., Ellis, P.J., Garman, E., Gonzalez, A., Sauter, N.K., Phizackerley, R.P., et al. (2002). Blu-Ice and the Distributed Control System: software for data acquisition and instrument control at macromolecular crystallography beamlines. J. Synchrotron Radiat. *9*, 401–406.

Momb, J., Wang, C., Liu, D., Thomas, P.W., Petsko, G.A., Guo, H., Ringe, D., and Fast, W. (2008). Mechanism of the quorum-quenching lactonase (AiiA) from *Bacillus thuringiensis*. 2. Substrate modeling and active site mutations. Biochemistry *47*, 7715–7725.

Murshudov, G.N., Skubák, P., Lebedev, A.A., Pannu, N.S., Steiner, R.A., Nicholls, R.A., Winn, M.D., Long, F., and Vagin, A.A. (2011). REFMAC5 for the refinement of macromolecular crystal structures. Acta Crystallogr. D Biol. Crystallogr. *67*, 355–367.

Mysinger, M.M., and Shoichet, B.K. (2010). Rapid context-dependent ligand desolvation in molecular docking. J. Chem. Inf. Model. *50*, 1561–1573.

Sali, A., and Blundell, T.L. (1993). Comparative protein modelling by satisfaction of spatial restraints. J. Mol. Biol. *234*, 779–815.

Sherman, W., Day, T., Jacobson, M.P., Friesner, R.A., and Farid, R. (2006). Novel procedure for modeling ligand/receptor induced fit effects. J. Med. Chem. *49*, 534–553.

Spellberg, B. (2014). The future of antibiotics. Crit. Care *18*, 228.

Stadler, M., and Dersch, P. (2016). How to Overcome the Antibiotic Crisis (Springer).

The PyMOL Molecular Graphics System (2018). The PyMOL Molecular Graphics System, Version 2.1.0 (Schrödinger LLC).

Winn, M.D., Ballard, C.C., Cowtan, K.D., Dodson, E.J., Emsley, P., Evans, P.R., Keegan, R.M., Krissinel, E.B., Leslie, A.G.W., McCoy, A., et al. (2011). Overview of the CCP4 suite and current developments. Acta Crystallogr. D Biol. Crystallogr. *67*, 235–242.

Wu, Z., Kan, S.B.J., Lewis, R.D., Wittmann, B.J., and Arnold, F.H. (2019). Machine-learning-assisted directed protein evolution with combinatorial libraries. Proc. Natl. Acad. Sci. U S A *116*, 8852–8858.

Xue, B., Chow, J.Y., Baldansuren, A., Yap, L.L., Gan, Y.H., Dikanov, S.A., Robinson, R.C., and Yew, W.S. (2013). Structural evidence of a productive active site architecture for an evolved quorum-quenching GKL lactonase. Biochemistry *52*, 2359–2370.

Yew, W.S., and Gerlt, J.A. (2002). Utilization of L-ascorbate by *Escherichia coli* K-12: assignments of functions to products of the yjf-sga and yia-sgb operons. J. Bacteriol. *184*, 302–306.

STAR★METHODS

KEY RESOURCES TABLE

REAGENT or RESOURCE	SOURCE	IDENTIFIER
Bacterial and Virus Strains		
Escherichia coli strain BL21(DE3) (Acella)	EdgeBio	36795
Chemicals, Peptides, and Recombinant Proteins		
N-butyryl-DL-homoserine lactone (C4-HSL)	Sigma-Aldrich	09945
N-hexanoyl-DL-homoserine lactone (C6-HSL)	Sigma-Aldrich	09926
N-heptanoyl-DL-homoserine lactone (C7-HSL)	Sigma-Aldrich	10939
N-octanoyl-DL-homoserine lactone (C8-HSL)	Sigma-Aldrich	10940
N-decanoyl-DL-homoserine lactone (C10-HSL)	Sigma-Aldrich	17248
N-dodecanoyl-DL-homoserine lactone (C12-HSL)	Sigma-Aldrich	17247
N-(3-oxohexanoyl)-L-homoserine lactone (3-oxo-C6-HSL)	Sigma-Aldrich	K3007
N-(3-oxooctanoyl)-L-homoserine lactone (3-oxo-C8-HSL)	Sigma-Aldrich	O1764
N-(3-oxodecanoyl)-L-homoserine lactone (3-oxo-C10-HSL)	Sigma-Aldrich	O9014
N-(3-oxododecanoyl)-L-homoserine lactone (3-oxo-C12-HSL)	Sigma-Aldrich	O9139
Geobacillus kaustophilus lactonase	This paper	UniProtKB: Q5KZU5
Deposited Data		
Structure of *Geobacillus kaustophilus* lactonase, Y99P mutan	This paper	PDB: 6JSS
Structure of *Geobacillus kaustophilus* lactonase, Y99P/D266N double mutant with bound 3-oxo-C8-HSL	This paper	PDB: 6JST
Structure of *Geobacillus kaustophilus* lactonase, Y99C/D266N double mutant	This paper	PDB: 6JSU
Structure of *Geobacillus kaustophilus* lactonase, wild-type with Zn^{2+}	(Xue et al., 2013)	PDB: 4H9U
Recombinant DNA		
Modified pET-15b	(Yew and Gerlt, 2002) Novagen	69661
Software and Algorithms		
PLOP	(Sherman et al., 2006)	http://www.jacobsonlab.org/plop_manual/plop_overview.htm
SPHGEN	(Kuntz et al., 1982)	http://dock.compbio.ucsf.edu/Contributed_Code/sphgen_cpp.htm
DOCK	(Mysinger and Shoichet, 2010)	http://dock.compbio.ucsf.edu/
XDS	(Kabsch, 2010)	http://xds.mpimf-heidelberg.mpg.de
CCP4	(Winn et al., 2011)	http://www.ccp4.ac.uk
PHASER	(McCoy et al., 2007)	https://www.phaser.cimr.cam.ac.uk
REFMAC	(Murshudov et al., 2011)	https://www2.mrc-lmb.cam.ac.uk/groups/murshudov/content/refmac/refmac.html
Phenix	(Adams et al., 2010)	http://www.phenix-online.org

(*Continued on next page*)

Continued

REAGENT or RESOURCE	SOURCE	IDENTIFIER
Coot	(Emsley et al., 2010)	http://www2.mrc-lmb.cam.ac.uk/personal/pemsley/coot
MolProbity	(Chen et al., 2010)	http://molprobity.biochem.duke.edu
PyMOL	Schrödinger LLC	https://www.pymol.org
Prism	GraphPad Software	https://www.graphpad.com/scientific-software/prism/

LEAD CONTACT AND MATERIALS AVAILABILITY

Further information and requests for resources and reagents should be directed to and will be fulfilled by the lead contact, Wen Shan Yew (bchyws@nus.edu.sg). Reagents generated in this study will be made available on request, but we may require a payment and/or a completed Materials Transfer Agreement if there is potential for commercial application.

EXPERIMENTAL MODEL AND SUBJECT DETAILS

GKL constructs were expressed in *Escherichia coli* strain Acella (EdgeBio).

METHOD DETAILS

Construction of Virtual Chemical Library

The virtual library is composed of 9 AHL compounds including C4-HSL, C6-HSL, C8-HSL, C10-HSL, C12-HSL, 3-oxo-C6-HSL, 3-oxo-C8-HSL, 3-oxo-C10-HSL and 3-oxo-C12-HSL. For each compound, its high-energy intermediate (HEI) was extracted from a previously described HEI docking library (Fan et al., 2013; Hermann et al., 2006, 2007), and used in the docking.

Materials

The following acyl homoserine lactones were purchased from Sigma-Aldrich - *N*-butyryl-DL-homoserine lactone (C4-HSL), *N*-hexanoyl-DL-homoserine lactone (C6-HSL), *N*-heptanoyl-DL-homoserine lactone (C7-HSL), *N*-octanoyl-DL-homoserine lactone (C8-HSL), *N*-decanoyl-DL-homoserine lactone (C10-HSL), *N*-dodecanoyl-DL-homoserine lactone (C12-HSL), *N*-(3-oxohexanoyl)-L-homoserine lactone (3-oxo-C6-HSL), *N*-(3-oxooctanoyl)-L-homoserine lactone (3-oxo-C8-HSL), *N*-(3-oxodecanoyl)-L-homoserine lactone (3-oxo-C10-HSL) and *N*-(3-oxododecanoyl)-L-homoserine lactone (3-oxo-C12-HSL). The chemical structures of all substrates tested are represented in Figure S1. All reagents were of the highest quality grade commercially available.

GKL Point Mutant Prediction and Molecular Docking

The crystal structure of GKL WT (PDBID: 4H9U) (Xue et al., 2013) was used as the template for *in silico* mutagenesis and molecular docking. A total of 99 residues were selected for point mutation generation, with each residue substituted into 19 other residue types independently. The sidechain conformations of the mutated residue and neighboring residues within 10 Å distance were predicted using the "side chain prediction" protocol in Protein Local Optimization Program (PLOP) (Sherman et al., 2006). For the resulting 1882 structures (the one solved for the wild-type and the 1881 predicted for the mutants), spheres and grids were generated prior to docking. 45 matching spheres serving to orient database compounds in the site were generated by augmenting the ligand-derived spheres with the receptor-derived spheres using the program SPHGEN (Kuntz et al., 1982). Docking screens were performed with DOCK version 3.6 (Mysinger and Shoichet, 2010). The docked compounds were ranked by the docking energy that is the sum of van der Waals, Poisson-Boltzmann electrostatic, and ligand desolvation penalty terms.

Overexpression and Purification of GKL

The cloning, expression and protein purification of the gene encoding GKL (GI: 56420041) was previously reported (Chow et al., 2010). All the mutant and wild-type GKLs were expressed and purified using the same protocol. Briefly, GKL constructs were made by cloning the coding sequences for wild-type and mutant GKLs into a modified pET-15b vector (Novagen) with an N-terminal tag of 10 instead of the usual 6 histidines. These constructs were expressed in Escherichia coli strain Acella (EdgeBio). Transformed cells were grown at 37°C in LB broth (supplemented with 100 μg/ml ampicillin) to an optical density of 0.6 at 600 nm, and isopropyl D-thiogalactopyranoside (0.1 mM) was added to induce protein expression for 16 h. The cells were harvested by centrifugation, resuspended in binding buffer (5 mM imidazole, 0.5 M NaCl, 20 mM Tris-HCl, pH 8.0), and lysed by sonication. The lysate was cleared by centrifugation, and the His-tagged protein was purified using a column of chelating Sepharose Fast Flow (GE Healthcare) charged with Ni2+. Cell lysate was applied to the column in binding buffer, washed with buffer containing 100 mM imidazole, 0.5 M NaCl, 20 mM Tris-HCl, pH 8.0, and eluted with 100 mM L-histidine, 0.5 M NaCl, 20 mM Tris-HCl, pH 8.0. The purified GKLs were dialyzed against storage buffer (100 mM NaCl, 20 mM Tris-HCl, pH 8.0) containing 0.1 mM 2,2'-bipyridyl followed by dialysis in storage buffer

to remove excess 2,2'-bipyridyl. Then, the protein solution was dialyzed against storage buffer containing 0.1 mM $ZnCl_2$ followed by dialysis in storage buffer to remove excess $ZnCl_2$. The concentrations of dialyzed GKLs were determined by their absorbance at 280 nm.

Biophysical Characterization of GKL

Size, oligomeric state and thermostability of purified wild-type GKL and selected mutants were measured with UNcle, an instrument manufactured by Unchained Labs, with recommended settings by the manufacturer (Table S3). Nine microliters of samples (10 mg/ml, in triplicates) were characterized firstly by dynamic light scattering at 25°C, followed by simultaneous static light scattering at 266 and 473 nm while heating the samples up from 25 to 95°C at 0.3°C/min.

Kinetic Assays of Lactonase Activity

The lactonase activities of wild-type GKL and its mutants were assayed by a continuous spectrophotometric pH indicator assay (Go et al., 2018), which measures the color change of m-cresol purple solution from purple to yellow (Figure S2), using a Biotek Synergy HT microplate reader to track the absorbance at 577 nm. This type of pH sensitive colorimetric assay has been routinely used in enzyme kinetics studies (Chapman and Wong, 2002). Briefly, the assay (50 μL at 37°C) contained 2.5-20 μM GKL, 2.5 mM bicine buffer, pH 8.3, 0.08 mM cresol purple (ε = 12,500 $M^{-1}cm^{-1}$ at 577 nm), and 0.025-5.0 mM AHL substrate dissolved in DMSO. Regardless of substrate concentration, the final concentration of organic solvent DMSO was maintained at 1%. We performed initial scouting assays for the different enzyme/substrate combinations to ensure the change in absorbance could be well captured and was almost linear within the first 5 min of the reaction. Initial rates (v_o) were corrected for the background rate of spontaneous substrate hydrolysis in the absence of enzyme. The GKL mutant was determined to be active when the rate of AHL hydrolysis is greater than 3x the background rate of nonenzymatic hydrolysis. Background rate of substrate nonenzymatic hydrolysis varied among different substrates and concentrations tested but was typically less than 30 milli-absorbance units/min and significantly below observed catalytic rates. The kinetic parameters were determined by fitting the initial rates to the Michaelis-Menten equation using Prism (Graphpad). Each assay was conducted 1-3 times depending on the quality of the data obtained, as judged by the standard deviations of the fitted kinetic parameters (Table S2).

Crystallization and Structure Solution of GKL Mutants

GKL mutants Y99C/D266N, Y99P and Y99P/D266N were crystallized under similar conditions as described before (Chow et al., 2010; Xue et al., 2013). Briefly, protein stocks were diluted to 25 mg/ml with the storage buffer to obtain working solutions. Those for Y99C/D266N and Y99P/D266N were doped with oxo-C8-HSL to a final concentration of 12.5 mM. The working solutions were mixed in a 1:1 ratio with the precipitant (17% w/v PEG 20000, 0.10 M Tris-HCl, pH 8.5, 0.10 M $MgCl_2$) and incubated at 25 degrees. Crystals obtained this way were soaked in a cryoprotectant (the precipitant supplemented with 30% glycerol) with or without oxo-C8-HSL, according to its presence/absence during crystallization, before being flash frozen. Diffraction data were collected at the MX1 and MX2 beamlines of the Australian Synchrotron, part of ANSTO, and made use of the Australian Cancer Research Foundation (ACRF) detector (Aragão et al., 2018; Cowieson et al., 2015; McPhillips et al., 2002). Data processing, structure solution and refinement, model building and validation, and figure generation were all conducted as previously reported (The PyMOL Molecular Graphics System, 2018; Adams et al., 2010; Chen et al., 2010; Emsley et al., 2010; Kabsch, 2010; McCoy et al., 2007; Murshudov et al., 2011; Winn et al., 2011). Briefly, data were indexed, scaled and merged in XDS (Kabsch, 2010), and converted to mtz format with the CCP4 package (Winn et al., 2011). Structure solution was achieved by molecular replacement in PHASER (McCoy et al., 2007). The model generated by PHASER was subject to repetitive rounds of refinement in REFMAC (Murshudov et al., 2011) or Phenix (The PyMOL Molecular Graphics System, 2018; Adams et al., 2010), followed by manual building in Coot (Emsley et al., 2010). Model quality was constantly monitored using MolProbity (Chen et al., 2010). Finalized models were used to generate structure-related figures in PyMOL (Schrödinger LLC).

QUANTIFICATION AND STATISTICAL ANALYSIS

Kinetic parameters for the hydrolysis of AHLs by wild-type and mutant GKLs were determined by fitting the initial rates of hydrolysis to the Michaelis-Menten equation using Prism (Graphpad). Each assay was conducted 1-3 times depending on the quality of the data obtained, as judged by the standard deviations of the fitted kinetic parameters (Table S2).

DATA AND CODE AVAILABILITY

Data Resources

The coordinates reported here have been deposited into the Protein Data Bank with PDB codes listed in Table 1.

Software Availability

This study did not generate new software. All software used in this study has been previously published and is publicly available.